Embedded printing of hydrogels and watery suspensions of cells in patterned granular baths.

Running title: Printing of suspensions and hydrogels in granular baths.

Authors: Vasileios D. Trikalitis, Julia Perea Paizal, Vincent Rangel, Fabian Stein and Jeroen Rouwkema*

University of Twente Faculty of Engineering Technology, Department of Biomechanical Engineering, Vascularization Lab, Technical Medical Centre, Drienerlolaan 5, 7522NB Enschede, Overijssel, NL

VDT: v.trikalitis@utwente.nl, phone +31534894848

JPP: julia.pereapaizal@gmail.com, phone +31 53 4894855

VR: v.rangel@iamfluidics.com, phone +31 53 4894855

FS: fabianstein@gmx.de, phone +31 53 4894855

JR: j.rouwkema@utwente.nl, phone +31 53 489 2892

Corresponding author*

Jeroen Rouwkema Dr.Ir.

Keywords: 3D bioprinting, embedding baths, granular media, granular inks, microgels, tissue a

Abstract

Bioprinting within support media has emerged as the superior alternative to conventional extrusion printing. Not only because it allows for more freedom over the shapes that can be printed, but also because it allows for the printing of inks that would not retain shape fidelity in freeform deposition such as watery liquids. Apart from functioning as mechanical support during embedded printing, hydrogel microparticle support media can provide the unique advantage of offering distinct chemotactic cues to cells printed in the baths by varying the composition of the hydrogel microparticles. There is great potential in compartmentalized granular baths consisting of different hydrogel particle materials in the field of tissue engineering, as these allow for the local inclusion of properties or cues to guide tissue development. In this work, we present a method to create compartmentalized embedding baths by printing multiple granular hydrogel materials that are widely used in tissue engineering. After adapting the volume fraction (ϕ_p) of the particles in the bath, we print within them using both inks composed of hydrogel or of cells and other particles suspended in watery liquid. Our process consists of three steps: First the hydrogel microparticles are packed at a ϕ_p that allows them to be extruded while being reversibly jammed, facilitating the localized deposition of the granular media to form a compartmentalized bath. Then, each granular media is deposited in succession to create a packed suspension compartment, and by adding liquid post deposition, ϕ_p is reduced to allow for embedded printing. Finally, we demonstrate the printing of multiple inks within the compartmentalized embedding bath, and highlight the distinct differences between using inks composed of hydrogels or inks composed of particles suspended in watery liquid. This approach combines the advantages of embedded printing through the use of granular media with the added ability to pattern multiple bioactive granular materials to locally affect the behaviour of cells printed within the bath. We expect that this workflow will allow researchers to create spatially

compartmentalized, customized bioactive embedding baths, that allow for the embedded printing of inks composed of hydrogels, cells and other particles adapted to their need.

Impact Statement:

While single phase embedding baths allow for the 3D printing of low viscosity inks and particle suspensions, the inability to compartmentalize them is an obstacle in creating a tissue-like spatial hierarchy. Current approaches based on hydrogel microparticles in the context of 3D printing either use a high particle fraction to create granular inks, that cannot function as embedding baths, or too low particle fraction where they function as granular baths but do not retain shape fidelity and are thus not printable. We present a process of particle suspensions that allows both for creating compartments and printing within them, creating multi-material regions with similar embedding properties. Therefore, future embedded granular printing approaches can achieve higher spatial chemotactic complexity and control.

1. Introduction:

Additive manufacturing offers the potential for scalable, automated and standardized production of tissues for medical applications[1]. Although different bioprinting methods have been developed such as vat polymerization (also known as Stereolithography (SLA))[2] and inkjet bioprinting[3], extrusion bioprinting[4] has been amongst the most popular techniques due to the broad variety of available inks and the relatively low costs of the equipment[5]. 3D bioprinting within support media, commonly known as embedded printing, has triggered a paradigm shift in conventional extrusion 3D bioprinting[6]. This is due to the unprecedented freedom of design that is offered in embedded printing, compared to standard Layer-by-Layer fabrication.

Embedding baths can be distinguished between 1) shear thinning bulk hydrogels[7-8] such as xanthan gum, 2) highly viscous yield stress fluids such as silicone elastomers[9], and 3) granular media that comprise of individual particles within a liquid phase at a high particle volume fraction(ϕ_p)[10] with materials such as gelatin[11], carbopol[12] and agar microgels[13]. The first demonstration of writing within a granular media, utilized Carbomer microgels as the particle phase of the embedding bath. These were suspended in water in order to achieve the shear thinning properties necessary for the suspension to function as an embedding bath[10]. There have since been reports of different materials used as granular baths, ranging in shape from amorphous[14] to spherical[15], and consisting of different compositions[16,17].

Hydrogel microparticles have shown great potential in biomedical applications[18], whether they function as cell carriers, controlled drug delivery moieties, chemotactic stimulators or cell capsules[19]. Through microfluidic production, hydrogel particles can be tailored to imitate specific tissue environments in terms of mechanical and chemotactic cues[20]. Scalable fabrication of hydrogel microparticles has already been demonstrated with a variety of methods[21-24], and therefore applications that demand high volumes, such as granular 3D printing inks[25-29], or granular embedding baths[10,14,15,30] are achievable for industrial scale applications.

A necessary property for a support material to function as an embedding bath is the capacity to thin when sheared, but thicken when shear is removed. These shear thinning and shear recovery properties are termed as thixotropy[31]. It is important to highlight that it is the gradual change of viscosity under shear that distinguishes thixotropic behavior compared to a sudden viscosity change due to irreversible jamming or unjamming[31]. A homogenous suspension of spherical particles, with no significant repulsive or attractive particle to particle interaction, can demonstrate thixotropic properties between

$0.5<\phi_p<\sim0.8$, which are a prerequisite for both granular inks and granular embedding baths[32]. Both particle composition and interstitial liquid composition can change particle to particle interactions, and can therefore affect the jamming and unjamming transition of the suspension[33,34]. However, the shear thinning and shear recovery of a particle suspension remains greatly determined by the volume fraction approximating the jamming regime[32]. So far, the processing of hydrogel granular media for embedded printing applications involves pouring the particle suspension into a container, and removing the water after sedimentation or centrifugation to attain the proper ϕ_p before performing embedded printing[10,13,15,35].

In a separate development, hydrogel microparticles have been used to prepare granular inks for extrusion printing. In this case, the microgels are generally jammed at a very high ϕ_p using vacuum filtration[23,25,36-40], centrifugation[41], solvent evaporation[42], or a combination of the aforementioned. Resuspending such a granular ink results in particle agglomerates as shown in [25,36], unless the hydrogel microparticles are annealed and thus the ink retains its fidelity[25]. Packing particles at a high ϕ_P as an injectable slurry which undergoes a secondary covalent inter-particle crosslinking step to form a structurally stable scaffold with interconnected porosity resulting from imperfect packing of spherical microgel, has been termed as a Microporous Annealed Particle Scaffold (MAPS)[27]. There are reports of MAPS that accelerate wound healing and tissue formation[27,43], modulate cell activity[44],and when combined with spatial control, cells can respond to the different chemotactic cues presented by both the particles and the interstitial material[45,46].

Printing of granular inks allows for the spatial design of jammed hydrogel microparticle suspensions. While initially ϕ_P was not investigated, it has become increasingly clear that accurately determining the ϕ_P [47], and most importantly handling the hydrogel microparticles in a manner that is reproducible[48], determines whether the particle suspension will behave as an ink, an embedding bath or an intermediate phase. Here we present a method where we carefully control ϕ_p of hydrogel microparticle formulations so that they can function both as an extrudable material, and as an embedding bath. We extrude reversibly jammed particles at an ink ϕ_p in a petri dish, dilute them via medium addition to a ϕ_p that allows functioning as an embedding bath, and then print cell suspensions within them. With the method presented, it is possible to utilize within a single system injectability and embedding bath properties, by manipulating the volume fraction.

2. Methods

2.1 Dry particle suspensions preparation

Corning® Collagen Coated Microcarriers (Corning) were used as the solid cell carriers for the bioactive granular inks and bath experiments. The dry particle powder was weighted and placed into a 50ml falcon tube. Then water, or MSC medium in the case of cell culture, was added supplemented with a final concentration of 12%v/v Iodixanol (STEMCELL technologies).

2.2 Hydrogel particles preparation

Alginate particles were fabricated using in-air microfluidics as described previously[22]. Briefly low viscosity 80-120cP sodium Alginate (WAKO PURE) was dispersed in water at a 1% w/v concentration under continuous stirring until dissolution and was used as the droplet train polymer jet. As a crosslinker jet an aqueous solution of 0.2M CaCl 10% EtOH was used. Both solutions were jetted through 75 and 100micron nozzles, and the alginate solution was vibrated to achieve controlled breakup. This resulted in particles with a diameter of 100 and 150μm for each nozzle. All the ejected material was collected in a 50ml falcon tube, resulting in a dilute alginate particle suspension. For the

alginate particle suspensions, alginate particles were washed 3 times with water and resuspended in medium for cell culture (or water for non cell experiments) with the addition of Iodixanol at 12% v/v concentration in order to have a density matched suspension. As hydrogel cell carriers, alginate particles with a gelatin coating were used, provided generously by IamFluidics B.V.

2.3 Preparation of particle suspension baths for bioprinting.

The hydrogel particles of experimental section 2.2 were immersed in 70% ethanol for 30 minutes, and then suspended in PBS while being exposed to UV light overnight for sterilization. The particles were left to sediment overnight in 50ml falcon tubes, after which the PBS supernatant was removed. Before extrusion, all hydrogel and solid particles were resuspended in MSC medium supplemented with 12% iodixanol and then strained with a 70 micron Cell strainer (Greiner) via sedimentation. After ensuring that there was no more droplet formation at the bottom of the cell strainer, the suspension was considered closely packed (ϕ~0.74). Then it was scooped with a stainless steel spatula into a 30ml luer lock syringe barrel (BD PLASTIPAK), where the plunger had been removed, as illustrated in Figure 1B. To prevent loss of material and simplify workflow, a luer lock red cap (BRAUN) was attached on the syringe after removing the plunger. After transferring of the suspension, the plunger was reattached and the syringe was gently tapped to bring the particle suspension closer to the plunger. In order to ensure adequate packing of the particles, the syringe was placed on a vortex up-side down to mechanically pack the particles at the plunger side. Finally, the luer cap was removed and the printing needle was attached. In the case of a smaller printer syringe module, a female/female luer lock adapter (CELLINK) can be used to transfer the suspension.

2.4 Cell culture and preparation of cell suspension inks.

GFP-Expressing Human Bone Marrow-Derived Mesenchymal Stromal Cells (GFP-MSCs; Angio-Proteomie, cAP-0050GFP) were used. These were seeded in a standard culture flask at a density of 5000-10000 cells/cm^2 and cultured in Dulbecco's Modified Eagle Medium supplemented with 10% FBS and 1% Pen/Strep (MSC medium). When the cells reached ~80% confluence, trypsin/EDTA was used to detach the cells. Detached cells were resuspended and transferred to a 50 mL tube which was centrifuged at 300G for three minutes. The supernatant was aspirated and one mL of corresponding medium was added. Finally, the cells were counted using a counting chamber and were resuspended in MSC medium containing 12% Optiprep at a cell concentration of 2*10^5 cells/ml. A 1 mL syringe (Luer-lock Plastipak, BD) was loaded with the cell suspension and used for 3D printing. The syringe was loaded using a 18G sterile nozzle to aspirate the cell suspension ink.

2.5 Hydrogel ink

For the hydrogel ink, Xanthan gum powder (11138-66-2, Sigma) at 3% w/v concentration and fluorescent pink acrylic paint (22.934, Acrylics Vallejo) at 1% v/v were dispersed in water overnight, under constant stirring.

2.6 Particle suspension inks

For the emulsion ink, fluorescent pink acrylic paint (22.934, Acrylics Vallejo) at 10% v/v was dispersed in hot water and mixed overnight under constant stirring. For the iron suspension, iron (II) oxide (FeO) powder (400866, Sigma Aldrich) was dispersed in 12% Iodixanol solution (OptiPrep™, STEMCELL TECHNOLOGIES) in order to extend sedimentation time and allow for extrusion.

2.7 3D printing

The g-code was programmed in-house and optimized for the 3D printer that was used in this study (DR.INVIVO; ROKIT Healthcare). All g-codes were executed with 20mm/s speed. For suspension inks the E value (distance traversed by plunger) of the g-code was calculated using the formula $V_{object}=V_{dispensed}$ where $V_{object}=l_{object}\ \pi r_{OD}^2$ and $V_{dispensed}=E\pi r_{plunger}$ solving for E. This value is used as 100% fill volume of the cavity opened by the nozzle in the granular medium, and E150, E200 are those values multiplied by 1.5 and 2, respectively. For hydrogel inks, the inner diameter of the nozzle was used as the radius of the object to be printed.

2.8 Imaging

Microscopy images were taken using an EVOS FL (ThermoFisher Scientific) using brightfield microscopy and a GFP filter. Macroscopic pictures were taken using a DSLR camera in a photo booth illuminated with UV led light strips.

2.9 Statistical analysis

Analysis of variance (ANOVA) one way and post hoc Tukey's test with honestly significant difference (HSD) was performed on the raw date to determine the significance of differences between the resolution of hydrogel inks (3.1) and suspension in aqueous viscosity inks (3.2) . The denotation of ***p<0.001 was used to indicate the significance level where it was applicable. Two way ANOVA and Tukey test with honest significant difference (HST) was performed for the violin plot of section 3.2, corresponding to table 1. Statistical analysis of section 3.2 was not integrated into the plot, since it would negatively impact readability.

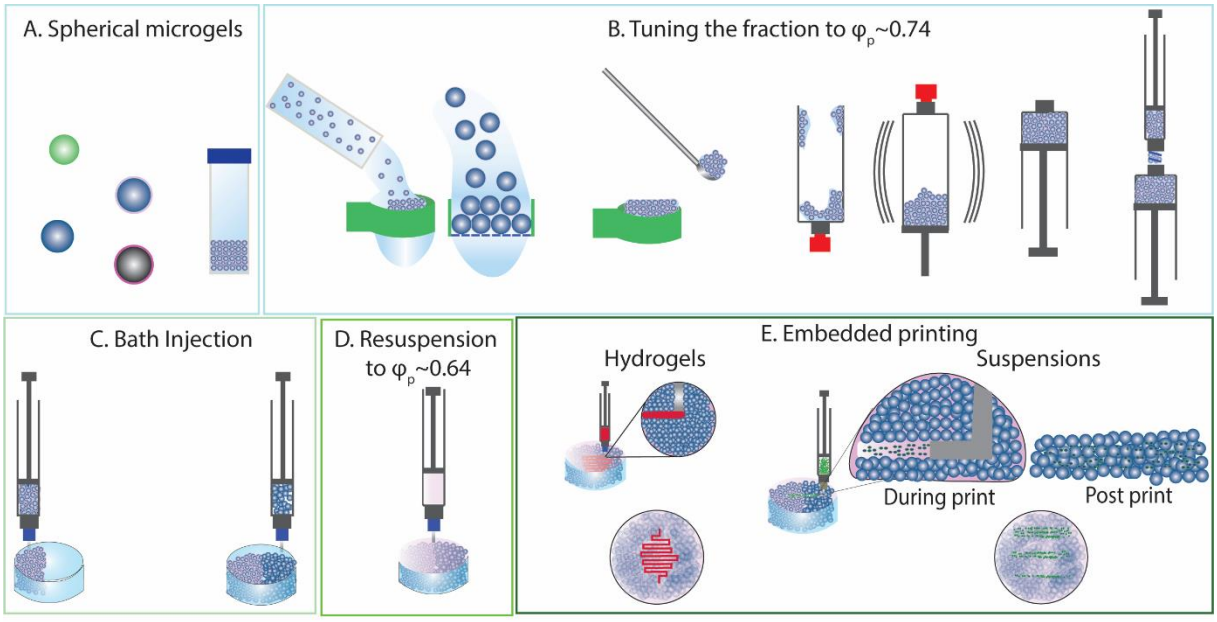

Figure 1: *Schematic summary of processing particle suspensions as injectables and 3D printing embedding baths.* ***(A)*** *Uniform spherical microgel suspensions of different sizes and compositions in water are produced using microfluidic production methods.* ***(B)*** *The particle dilute suspension is transferred onto a cell strainer with a mesh diameter smaller than the particle diameter. Thus the φ_p of the suspension is increased to ~0.74 (close packing) without compromising the hydrogel particles through vacuum or centrifuging. When there is no more liquid dripping from the cell strainer, the suspensions are transferred into a syringe container compatible with the 3D printing apparatus in such*

a way that volume fraction remains constant. For this, suspensions are scooped into a large syringe and the syringe is subsequently vibrated to force the suspension on the plunger of the syringe. Then the air is removed from the syringe by moving the plunger and the suspension is transferred to the printing syringe using a female to female Luer lock connector. ***(C)*** *The granular inks are subsequently injected into a petri dish, where multiple granular inks can be combined for the creation of compartments.* ***(D)*** *Then, a controlled amount of cell medium is added (10% of the total volume of particle suspension injected in the petri dish) in order to lower the particles φ_p to ~0.64 and gain embedding bath properties.* ***(E)*** *Hydrogel inks and particle suspensions can now be printed within the compartmentalized embedding bath.*

3. Experiment

3.1 Assessment and comparison of Alginate particles, Gelatin-coated Alginate particles, and collagen coated solid particles in terms of printability and embedding bath potential for the 3D printing of hydrogel inks.

4ml of each particle type were packed at ~0.74 ϕ_P as described in the methods section and Figure 1B and were injected onto a petri dish and 400µl of water was added gently on top to reach a ϕ_p ~0.64. Hydrogel particles were able to extrude, however solid carriers jammed irreversibly and could thus not be extruded. Therefore, the solid cell carriers were scooped with a spatula after packing. Xanthan hydrogel ink could be printed without a support bath, but this resulted in a poor printing resolution of 653 ± 28µm as the material spread out after extrusion due to its liquid behaviour. Apart from a poor resolution, this also resulted in poor shape fidelity due to the merging of subsequent lines in the corners (Figure 2.C. i and ii). Extrusion in the three different bath materials resulted in a better resolution of 545± 72µm, 522 ± 42µm and 493 ± 46µm respectively, as shown in Figure 2.B using violin plots. Shape fidelity was also better preserved due to the stabilizing effect of the bath as shown In Figure 2.C macroscopically and microscopically, and as shown in Figure S3 for a large 3D print with a complex shape. The microscopy images were used to assess the fidelity of the 3D print in each condition. In all cases, printing within the bath improved the fidelity of the ink. The particle opacity is another significant parameter as seen when the gelatin coated and uncoated alginate hydrogel particles are compared to the collagen coated solid particles (Figure 2.C (i-viii). Imaging both macroscopically and microscopically was significantly more challenging in the case of solid particles.

3.2 Printing and assessment of iron particle, pigment emulsion and MSC cell suspension inks in granular suspensions of Alginate hydrogel microparticles with different infill (E) values highlighting the impact of nozzle choice.

4ml of alginate hydrogel microparticle suspensions were injected in 35mm petri dishes and 400µL of water was added to the suspension to reach a ϕ_p~0.64 to enable embedded printing. Suspension inks of iron particles, GFP-MSC cells and pigment emulsion were printed with a 22G straight needle. Immediately after print, the printed lines were visible, especially in the case of the emulsion pigment (Figure 3.A.i), but they rapidly diffused to the surrounding area resulting in an amorphous mix (Figure 3.A.ii). This result occurred in all cases of particle suspension inks and was validated microscopically (Figure 3.A.iii-iv). Notably when a 90° bent needle was used, the printed lines retained their shape and size (Figure 3.B.i). Then in order to validate that this is a controlled process, the E value was increased in 50% intervals, resulting in a proportional increase of feature diameter, while retaining the overall shape (Figure 3.B.ii-x) for all variations of suspension inks. In order to validate that the particles are indeed suspended, different height focus points on the z axis of the same spot were imaged and contrast enhanced (Figure 3.C.i-vi). It is shown that the particles were trapped within the interstitial

space of the hydrogel particles in 3C. The feature diameter was quantified for each type of suspension ink, and all suspension inks showed similar resolution at E-value equal to 100% of the nozzle OD. The iron particles showed a significant increase in diameter of print when the flow rate was increased. They are notably smaller than the other two suspension ink particles, and thus this observed diameter increase can be correlated.

Table 1. *Two-Way ANOVA for figure 3.C with Tukey's test*

Overall ANOVA	*DF*	*Sum of Squares*	*Mean Square*	F *Value*	p *Value*
Ink type	2	2.9149E7	1.45745E7	556.64793	<0.0001
E-value	2	1.83062E7	9153094.35689	349.58692	<0.0001
Interaction	4	8342163.19858	2085540.79964	79.65369	<0.0001
Model	8	5.57973E7	6974666.50454	266.38556	<0.0001
Error	108	2827720.77216	26182.59974		
Corrected total	116	5.86251E7			

Ink type	*MeanDiff*	*SEM*	q *Value*	*Prob*	*Alpha*	*Sig*	*LCL*	*UCL*
Iron powder red emulsion	1010.20631	36.64284	38.98845	<0.0001	0.05	1	923.12614	1097.28648
GFP cells red emulsion	−91.32541	36.64284	3.52466	0.03751	0.05	1	−178.40558	−4.24524
GFP cells iron powder	−1101.53172	36.64284	42.51311	<0.0001	0.05	1	−1188.61189	−1014.45155

E-value	*MeanDiff*	*SEM*	q *Value*	*Prob*	*Alpha*	*Sig*	*LCL*	*UCL*
150 100	545.58105	36.64284	21.05645	<0.0001	0.05	1	458.50088	632.66122
200 100	966.21692	36.64284	37.2907	<0.0001	0.05	1	879.13675	1053.29709
200 150	420.63587	36.64284	16.23425	<0.0001	0.05	1	333.5557	507.71604

At the 0.05 level, the population means of Ink type are significantly different. At the 0.05 level, the population means of E-value are significantly different. At the 0.05 level, the interaction between Ink type and E-value are significantly different.

3.3 Demonstration of cell suspension ink printing in a printed, compartmentalized bath of alginate particles combined with alginate-gelatin coated particles.

2ml of Alginate particles and 2 ml of Gelatin coated Alginate hydrogel particles were printed opposite to each other in a 35mm petri dish in order to create a compartmentalized suspension and 400µL of MSC medium was added to reach a ϕ_p~ 64(Figure 4.A.i-ii). Then GFP-MSC cell suspension inks were printed across the compartmentalized embedding bath with a 90° bent 27G needle, spanning both regions of the bath at different E-values. In all cases the cells are trapped in the interstitial space between the particles in a linear format, and increasing the E-value increased both the number of the cells and the diameter of the line (Figure 4.B.i-ix). Due to the difference in the optical index of the Gelatin coated particles, the compartment borders are clearly visible (Figure 4.B.ii,v,ix). A few Gelatin coated alginate particles can be observed to be dragged along in the alginate particle area from the nozzle, but without disturbing the overall compartmentalization of the embedding bath and still retaining print fidelity (Figure 4.B.iii,vi,ix). As the alginate-gelatin coated particles allow for cell attachment and the alginate particles do not, the printed cells can potentially behave differently in the two compartments. Although this was not seen upon culture in this experiment, potentially due to the relatively low cell density after printing, a different proof-of-principle experiment where an ink consisting of cells suspended in 8 mg/ml fibrinogen was printed in a compartmentalized bath consisting of alginate particles combined with coated alginate particles did show a clear difference in behaviour of the cells within the two compartments (Figure S2).

Discussion

Embedding baths have enabled unprecedented control over the designs that can be 3D printed via extrusion bioprinting[6]. Due to the early stage development of the method, having its debut in 2015[10] the principal mechanisms and classifications that are necessary to be considered in order to ensure reproducibility are not yet elucidated. A first level of distinction is necessary when embedded printing is conducted regarding the ink type that is extruded within the bath as we showed in this study; whether the ink is a particle suspension such as cells in medium or a Newtonian fluid phase[8,49], a cell laden hydrogel that exhibits thixotropic properties such as GelMA[50], or an in-situ crosslinking material which would fall somewhere in between[15,51] (Figure S.2).

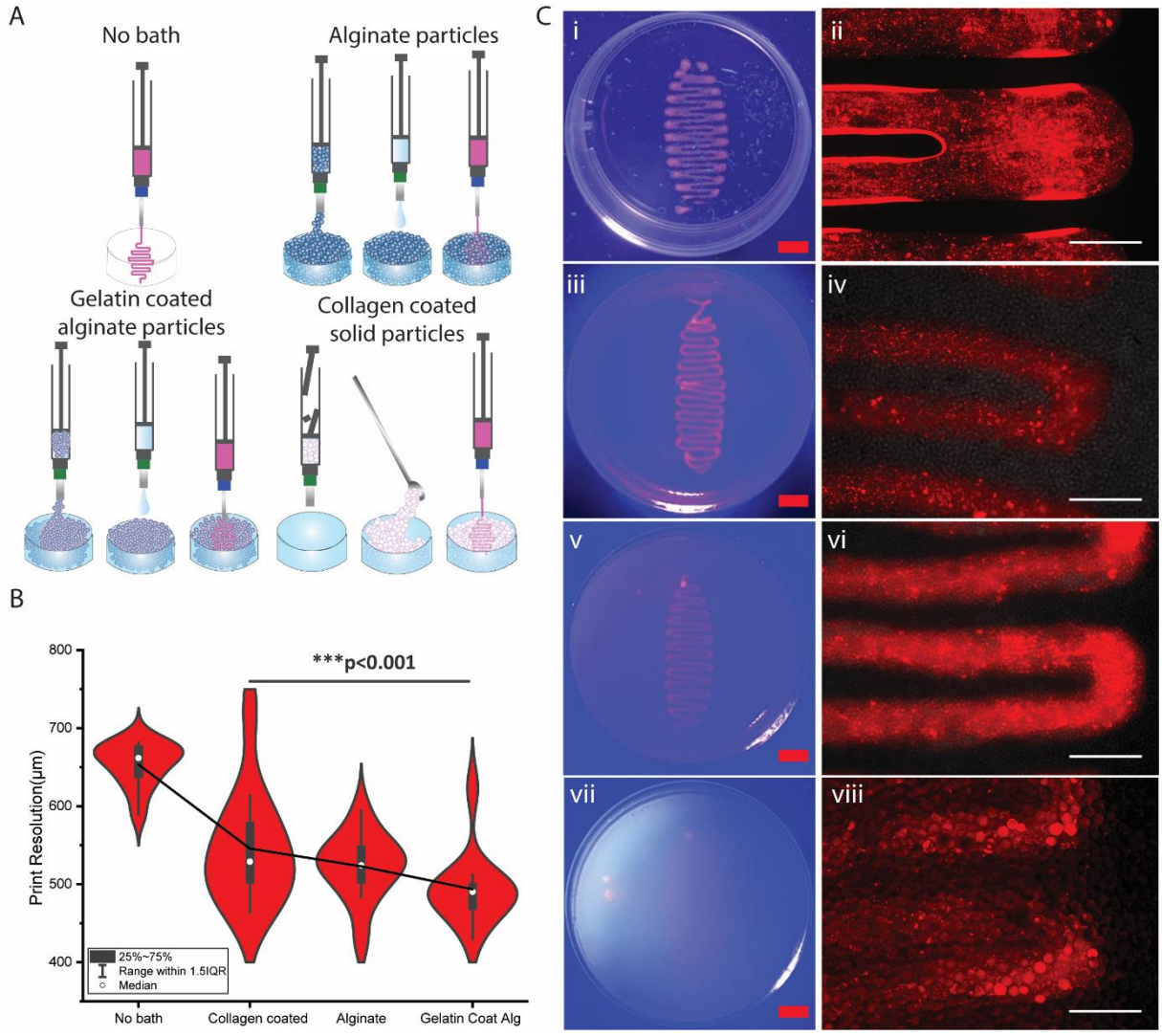

Figure 2: *Assessment of embedding bath potential for Alginate particles, Gelatin coated alginate hydrogel particles, and collagen coated solid carriers.* ***(A)*** *Workflow illustration for the loading of particles in the container, resuspension and 3D printing within it. Collagen coated solid carriers could not be printed, so they were scooped into the container.* ***(B)*** *Quantification of print resolution for the xanthan hydrogel ink, without a bath and in different embedding baths. Fidelity of shape increases by using a support bath in all cases compared to the control with a significant difference of p<0.001 (***) but no statistical significance compared between different baths.* ***(C) i,iii,v,vii*** *macroscopic images of the 3D printed ink within the bath. The opaque nature of the gelatin coated carriers makes imaging*

difficult. ***ii,iv,vi,viii*** *microscopic imaging of the xanthan ink, fidelity is visibly better when baths are used, both in resolution diameter but also in feature fidelity as noted in the sharp turns of the snake design. White scale bar=1mm Red scale bar=5mm.*

The second level of distinction is whether the printing of the ink of choice occurs in continuous viscoelastic hydrogel baths[7,8] or granular media[10,14,52]. When focused on granular media, the key parameters seem to be the particle size, particle type, particle to particle interaction, particle volume fraction and interstitial liquid phase. This can be observed in the vastly different results when carbopol EDT2020, a micelle particle <1 micron[53] is used. This embedding bath material allows for high fidelity printing with a straight needle, but does not allow the cell takeover of the interstitial space as can be observed in the literature[30,54]. In contrast, when microparticles of several tens of microns(>80μm) are used as an embedding bath, and thixotropic ink or in situ-crosslinking print fidelity is achieved, the embedding bath acts only as a mechanical support and patterning moiety, and the key interplay is between the cells and the ink used[51]. In order to combine the chemotactic potential of hydrogel microparticles, the desired outcome would be to allow the cells to directly interact with the particles of the embedding bath suspension.

We also demonstrated in our work that the embedded printing of particle suspension inks (including cell inks as they have been termed), is not possible with a straight nozzle when using embedding baths consisting of particles of >80μm suspended in water or medium. Modifying the interstitial liquid phase with a viscous polymer has been employed in order to assist fidelity[52], but then the problem of not allowing the cells to directly interact with the particle suspension reemerges and the particle suspension again mainly operates as a porogen and mechanical support. Moreover, modifying the interstitial phase of the embedding bath particle suspension creates a cascade of interactions for the mechanics of the particle suspension, which leads to a case by case workflow[55]. Our work demonstrates how to print suspension inks without altering the composition of the embedding bath, but rather alter the nozzle architecture to fit the ink behavior. The aforementioned parameters also apply to the injectability of the particle suspensions, since modifying the interstitial phase[55] or the particle shape and size[56], leads to a different rheological behavior.

Volume fraction has been identified as an important parameter[18] for the behavior of embedding baths, but it is in no case the only one. In our work we demonstrate that controlling the volume fraction, with uniform hydrogel particles with a size of 100 and 150μm, and an interstitial phase of water or cell medium, the particles can be injected into a container, and by adding liquid we can turn a granular ink into a granular embedding bath. We also demonstrate that a solid particle suspension at a similar particle fraction, simply does not work the same (Figure 2) thus highlighting the importance of particle type for this approach.

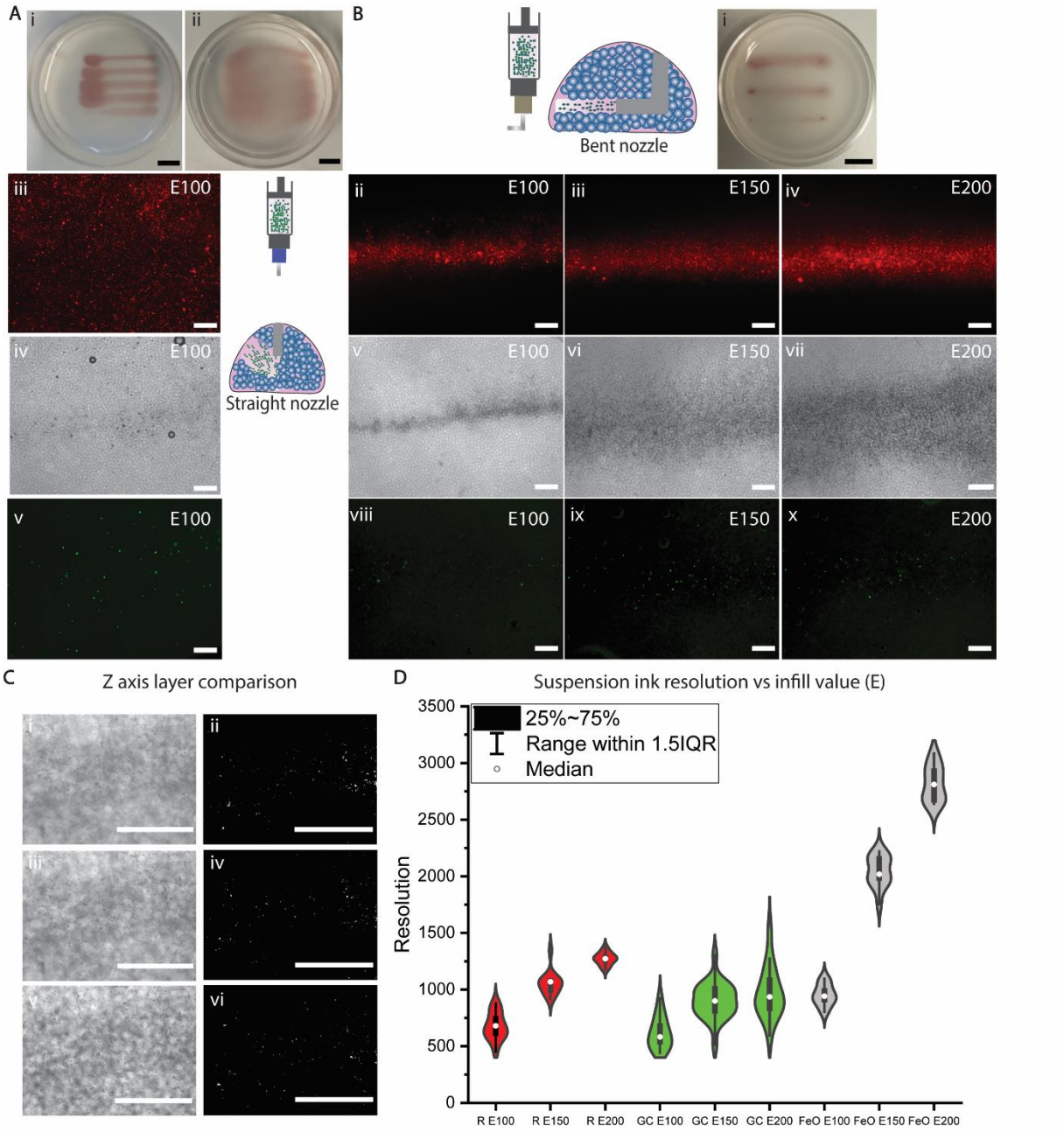

Figure 3: *Assessment of printing potential of suspension inks within granular embedding baths.* ***(A)*** *Using a straight nozzle for suspension inks results in loss of features after a few seconds of deposition* ***(i,ii)*** *and the result was consistent in every type of particle ink, as it was observed with emulsion pigment* ***(i)****, iron particles* ***(ii)*** *and GFP-MSCs* ***(iii)****.* ***(B)*** *Using a 27G 90º bent nozzle the feature is retained* ***(i)*** *and the diameter of features increases proportionately, to the E value for the emulsion ink* ***(i-iii)****, the iron particle ink* ***(iv-vi)*** *and the cell suspension ink* ***(viii-x)****. Both the E value and the type of ink differ in a statistically significant manner, as shown in Table 1.* ***(C)*** *The particles are suspended in 3D, throughout the embedding bath interstitial space as it was observed at different z levels* ***(i,iii,v)*** *and made clear when the contrast was enhanced* ***(ii,iv,vi)*** ***(D)*** *The printed lines of all suspension inks was quantified and compared across E value and particle ink type. Black scalebar 5mm, white scale bar=1mm*

Then we perform embedded printing and demonstrate the improvement in fidelity of a xanthan gum ink, while also highlighting the effect of particle opacity for imaging the target print. Even with a fluorescent pigment color the particle suspension hinders precise visualization with microscopy as shown in Figure 2C. Removing the suspension for imaging via dilution is possible, but then the structure will be subjected to perturbations and in the case of fragile structures, it will result in deformation. Matching the optical index of the particles with the interstitial fluid can be a solution but caution must be exercised in to not affect the rheological or chemotactic properties of the particle suspension.

The limitations in our study are present in four key areas. The first is that this workflow is reproducible for uniform, spherical, hydrogel particles. The uniformity of shape and size aspect is a prerequisite since that is how the ϕ_p can be estimated reproducibly for different materials[57]. Different shapes of particles result in different packing fractions[58] with the same methodology and thus will yield different results. Particle size is also directly correlated with the interstitial volume, and thus if the embedding bath particles are too large relatively to the ink particles, the suspension ink particles will flow through the gaps.

The second limitation is regarding the extrusion of the embedding bath particle suspension as inks. In our work, the flow of the particle suspension during injection is continuous but inconsistent, in the sense that due to pressure build up in the syringe, the particle suspension flows initially as more liquid like, and gradually a more jammed suspension exits the nozzle. Since the hydrogel particles during the injection phase have not deformed and agglomerated from the process, after complete extrusion of the particle suspension, the final ϕ_p will be the same as the ϕ_p in the syringe. To completely control the compartmentalization of the embedding baths, a controlled flow of reversibly jammed particles would be ideal but this has not been demonstrated in the literature so far. Thus, to the best of our knowledge we have not yet encountered 3D printing of granular suspensions and we hypothesize that this inconsistent flow has been encountered in literature when dense particle suspensions are extruded. Studies that do report granular hydrogel inks utilize “overjamming” via vacuuming[25], which might lead to a consistent flow of particles, but results in irreversibly jammed particles that cannot be resuspended to an embedding bath ϕ_P by just adding liquid.

The third limitation is present in the printing of suspension inks. In this study, the particles within the suspension inks are smaller than the particles that constitute the embedding bath. This makes it possible for the particles within the ink to flow through the interstitial spaces between the embedding bath particles when a standard nozzle is used. Our hypothesis for the fact that a 90^o bent nozzle allows the printing of suspension inks, is that a granular diffusion packing, similar to diffusion packing occurs[8]. The direction of the particle velocity and the direction of the embedding bath disturbance from the nozzle architecture combined is a determining condition for successful printing. This indicates that sheet shaped prints or volume shapes will be difficult or impossible to print with current approaches, regardless of whether a straight or a bent nozzle is used.

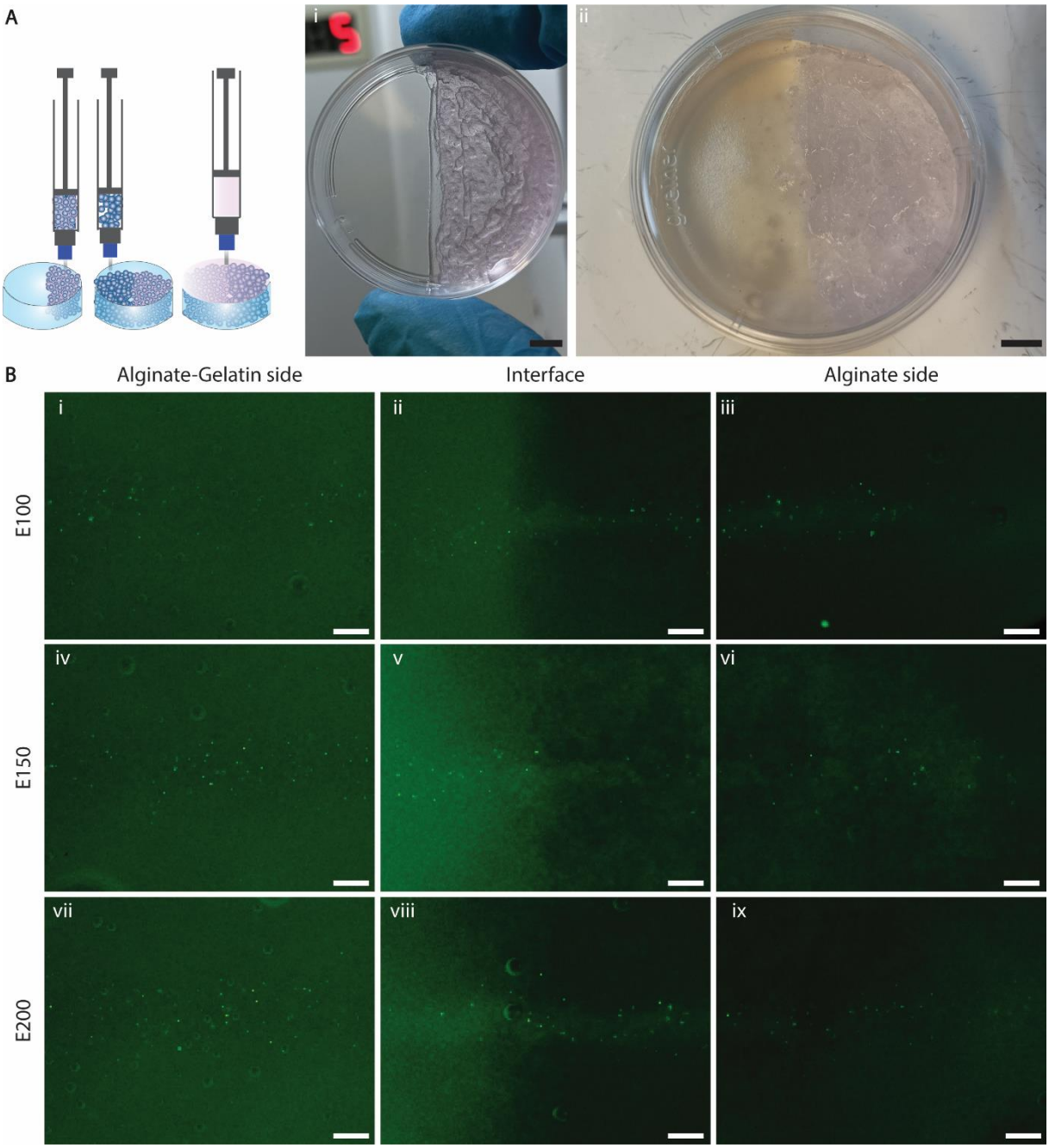

Figure 4: *Printing cell suspensions in compartmentalized baths.* ***(A)*** *Injection of Alginate hydrogel particles* ***(i)*** *and injection of Gelatin coated particles and resuspension with medium* ***(ii)*** *to prepare the compartmentalized embedding bath.* ***(B)*** *After GFP-MSCs suspension ink printing using a 27G 90° bent nozzle with different E values in the gelatin coated alginate particle side* ***(i,iv,vii)****, across the interface* ***(ii,v,viii)*** *and into the alginate particle side* ***iii,vi,ix****. Black scale bar 5mm, white scale bar 1mm.*

The final limitation is present in the medium change, fixation and staining processing that is necessary in most tissue engineering protocols. By definition, a particle suspension is dynamic and sensitive to the addition or subtraction of liquid volume. While we offer solutions for medium

change aimed for cell and tissue culture (S.1.), fixating and staining, which usually requires extensive washing steps, would necessitate that the printed tissue or structure would be robust enough to withstand the process. Simply put, if the tissue is too fragile to be removed from the suspension, it will be also fragile to be fixated, and stained (S.1). Thus, our method is useful for matured tissues and robust structures but would probably fall short for frangible assemblies.

Conclusions

Implementing the practice of a controlled volume fraction, Alginate and Gelatin coated Alginate hydrogel particles could be reversibly jammed and used as an extrudable ink to form embedding baths. Solid cell carriers could not be extruded due to clogging, but could still be used to form embedding baths. After marginally lowering the particle volume fraction to attain embedding bath properties, all investigated granular embedding bath materials allowed for reproducible embedded 3D printing of hydrogel inks and suspensions of cells or particles in watery liquid.. For suspension inks such as cell suspensions, iron powder suspensions or emulsions, for which the size of the particles in the ink was more than 10 times smaller than the size of the particles composing the embedding bath, a 90^{o} bent nozzle had to be used in order to achieve feature fidelity. The resolution of the printed lines was dependent on the outer diameter of the nozzle, but mainly on the amount of extruded ink which is connected to the infill volume or the E-value in the G-code of the printer. Notably, the embedding baths can become compartmentalized by printing the different bath particles at different positions. This allowed for the printing of cell suspensions spanning both compartments, thus offering spatial variations in the chemotactic cues that the printed cells experience. The proposed framework offers the potential to print suspension inks and hydrogel inks within compartmentalized embedding baths that can provide local chemotactic cues based on the bath design, which has the potential to locally control cell behaviour when printed cells are cultured within the embedding bath.

Acknowledgments:
Special thanks to Despina Liakopoulou for helping with the camera pictures for Figure 2.

Funding statement:

This project was funded by the European Research Council (ERC) under the European Union's Horizon 2020 Research and Innovation Programme (No. 861895)**.**

Conceptualization: VDT, JR; **Methodology**: VDT, FS; **Investigation**: VDT, JPP, VR, FS; **Formal Analyses**: VDT; **Funding Acquisition**: JR; **Project Administration**: VDT, JR; **Supervision**: JR; **Visualization**: VDT; **Original Draft**: VDT; **Review and Editing**: VDT, JPP, VR, FS, and JR.

Disclosure statement:

Vasileios D. Trikalitis is employed as a Product Innovation Manager in IamFluidics B.V. which produces hydrogel microparticles.

References

1. Mota C, Puppi D, Chiellini F, et al. Additive manufacturing techniques for the production of tissue engineering constructs. Journal of Tissue Engineering and Regenerative Medicine 2015;9(3):174-190, doi:https://doi.org/10.1002/term.1635
2. Chartrain NA, Williams CB, Whittington AR. A review on fabricating tissue scaffolds using vat photopolymerization. Acta Biomater 2018;74(90-111, doi:10.1016/j.actbio.2018.05.010

3. Ng WL, Huang X, Shkolnikov V, et al. Polyvinylpyrrolidone-based bioink: influence of bioink properties on printing performance and cell proliferation during inkjet-based bioprinting. Bio-Design and Manufacturing 2023;6(6):676-690, doi:10.1007/s42242-023-00245-3
4. Ramesh S, Harrysson OLA, Rao PK, et al. Extrusion bioprinting: Recent progress, challenges, and future opportunities. Bioprinting 2021;21(e00116, doi:https://doi.org/10.1016/j.bprint.2020.e00116
5. Ozbolat IT, Hospodiuk M, . Current advances and future perspectives in extrusion-based bioprinting. 2016;76(321-343, doi:10.1016/J.BIOMATERIALS.2015.10.076
6. McCormack A, Highley CB, Leslie NR, et al. 3D Printing in Suspension Baths: Keeping the Promises of Bioprinting Afloat. Trends in Biotechnology 2020;38(6):584-593, doi:10.1016/j.tibtech.2019.12.020
7. Patrício S, Sousa L, Correia T, et al. Freeform 3D printing using a continuous viscoelastic supporting matrix. Biofabrication 2020;12(doi:10.1088/1758-5090/ab8bc3
8. Trikalitis VD, Kroese NJJ, Kaya M, et al. Embedded 3D printing of dilute particle suspensions into dense complex tissue fibers using shear thinning xanthan baths. Biofabrication 2022;15(1), doi:10.1088/1758-5090/aca124
9. Muth JT, Vogt DM, Truby RL, et al. Embedded 3D Printing of Strain Sensors within Highly Stretchable Elastomers. Advanced Materials 2014;26(36):6307-6312, doi:https://doi.org/10.1002/adma.201400334
10. Bhattacharjee T, Zehnder SM, Rowe KG, et al. Writing in the granular gel medium. Science Advances 2015;1(8):e1500655, doi:doi:10.1126/sciadv.1500655
11. Bliley J, Tashman J, Stang M, et al. FRESH 3D bioprinting a contractile heart tube using human stem cell-derived cardiomyocytes. Biofabrication 2022;14(2):024106, doi:10.1088/1758-5090/ac58be
12. Nelson AZ, Kundukad B, Wong WK, et al. Embedded droplet printing in yield-stress fluids. 2020;117(5671-5679, doi:10.1073/PNAS.1919363117/SUPPL_FILE/PNAS.1919363117.SM04.MP4
13. Senior JJ, Cooke ME, Grover LM, et al. Fabrication of Complex Hydrogel Structures Using Suspended Layer Additive Manufacturing (SLAM). Advanced Functional Materials 2019;29(49):1904845, doi:https://doi.org/10.1002/adfm.201904845
14. Hinton TJ, Jallerat Q, Palchesko RN, et al. Three-dimensional printing of complex biological structures by freeform reversible embedding of suspended hydrogels. Science Advances 2015;1(9):e1500758, doi:doi:10.1126/sciadv.1500758
15. Lee A, Hudson AR, Shiwarski DJ, et al. 3D bioprinting of collagen to rebuild components of the human heart. Science 2019;365(6452):482-487, doi:doi:10.1126/science.aav9051
16. Kajtez J, Wesseler MF, Birtele M, et al. Embedded 3D Printing in Self-Healing Annealable Composites for Precise Patterning of Functionally Mature Human Neural Constructs. Advanced Science 2022;9(25):2201392, doi:https://doi.org/10.1002/advs.202201392
17. Noor N, Shapira A, Edri R, et al. 3D Printing of Personalized Thick and Perfusable Cardiac Patches and Hearts. Advanced Science 2019;6(11):1900344, doi:https://doi.org/10.1002/advs.201900344
18. Daly AC, Riley L, Segura T, et al. Hydrogel microparticles for biomedical applications. Nature Reviews Materials 2020;5(1):20-43, doi:10.1038/s41578-019-0148-6
19. Caldwell AS, Aguado BA, Anseth KS. Designing Microgels for Cell Culture and Controlled Assembly of Tissue Microenvironments. Adv Funct Mater 2020;30(37), doi:10.1002/adfm.201907670
20. Li W, Zhang L, Ge X, et al. Microfluidic fabrication of microparticles for biomedical applications. Chemical Society Reviews 2018;47(15):5646-5683, doi:10.1039/C7CS00263G
21. Kamperman T, Trikalitis VD, Karperien M, et al. Ultrahigh-Throughput Production of Monodisperse and Multifunctional Janus Microparticles Using in-Air Microfluidics. ACS Applied Materials & Interfaces 2018;10(28):23433-23438, doi:10.1021/acsami.8b05227
22. Visser CW, Kamperman T, Karbaat LP, et al. In-air microfluidics enables rapid fabrication of emulsions, suspensions, and 3D modular (bio)materials. Science Advances 2018;4(1):eaao1175, doi:doi:10.1126/sciadv.aao1175

23. Zhang H, Tumarkin E, Peerani R, et al. Microfluidic Production of Biopolymer Microcapsules with Controlled Morphology. Journal of the American Chemical Society 2006;128(37):12205-12210, doi:10.1021/ja0635682
24. Zhang Y, Yin P, Huang J, et al. Scalable and high-throughput production of an injectable platelet-rich plasma (PRP)/cell-laden microcarrier/hydrogel composite system for hair follicle tissue engineering. Journal of Nanobiotechnology 2022;20(1):465, doi:10.1186/s12951-022-01671-8
25. Highley CB, Song KH, Daly AC, et al. Jammed Microgel Inks for 3D Printing Applications. Advanced Science 2019;6(1):1801076, doi:https://doi.org/10.1002/advs.201801076
26. Hsu R-S, Chen P-Y, Fang J-H, et al. Adaptable Microporous Hydrogels of Propagating NGF-Gradient by Injectable Building Blocks for Accelerated Axonal Outgrowth. Advanced Science 2019;6(16):1900520, doi:https://doi.org/10.1002/advs.201900520
27. Griffin DR, Weaver WM, Scumpia PO, et al. Accelerated wound healing by injectable microporous gel scaffolds assembled from annealed building blocks. Nature Materials 2015;14(7):737-744, doi:10.1038/nmat4294
28. Hirsch M, Charlet A, Amstad E. 3D Printing of Strong and Tough Double Network Granular Hydrogels. Advanced Functional Materials 2021;31(5):2005929, doi:https://doi.org/10.1002/adfm.202005929
29. Zhang H, Cong Y, Osi AR, et al. Direct 3D Printed Biomimetic Scaffolds Based on Hydrogel Microparticles for Cell Spheroid Growth. Advanced Functional Materials 2020;30(13):1910573, doi:https://doi.org/10.1002/adfm.201910573
30. Bhattacharjee T, Gil CJ, Marshall SL, et al. Liquid-like Solids Support Cells in 3D. American Chemical Society: 2016.
31. Larson RG, Wei Y. A review of thixotropy and its rheological modeling. Journal of Rheology 2019;63(3):477-501, doi:10.1122/1.5055031
32. Mueller S, Llewellin EW, Mader HM. The rheology of suspensions of solid particles. Proceedings of the Royal Society A: Mathematical, Physical and Engineering Sciences 2010;466(2116):1201-1228, doi:doi:10.1098/rspa.2009.0445
33. Ancey C. Role of lubricated contacts in concentrated polydisperse suspensions. Journal of Rheology 2001;45(6):1421-1439, doi:10.1122/1.1413504
34. Maranzano BJ, Wagner NJ. The effects of interparticle interactions and particle size on reversible shear thickening: Hard-sphere colloidal dispersions. Journal of Rheology 2001;45(5):1205-1222, doi:10.1122/1.1392295
35. Shen EM, McCloskey KE, . Affordable, high-resolution bioprinting with embedded concentration gradients. 2021;21(doi:10.1016/J.BPRINT.2020.E00113
36. Muir VG, Prendergast ME, Burdick JA. Fragmenting Bulk Hydrogels and Processing into Granular Hydrogels for Biomedical Applications. J Vis Exp 2022;183), doi:10.3791/63867
37. Muir VG, Qazi TH, Weintraub S, et al. Sticking Together: Injectable Granular Hydrogels with Increased Functionality via Dynamic Covalent Inter-Particle Crosslinking. Small 2022;18(36):2201115, doi:https://doi.org/10.1002/smll.202201115
38. Qazi TH, Muir VG, Burdick JA. Methods to Characterize Granular Hydrogel Rheological Properties, Porosity, and Cell Invasion. ACS Biomaterials Science & Engineering 2022;8(4):1427-1442, doi:10.1021/acsbiomaterials.1c01440
39. Hoon Song K, Highley CB, Rouff A, et al. Complex 3D-Printed Microchannels within Cell-Degradable Hydrogels. 2018;28(1801331, doi:10.1002/ADFM.201801331
40. Prendergast ME, Davidson MD, Burdick JA, et al. A targeted rheological bioink development guideline and its systematic correlation with printing behavior. IOP Publishing: 2021.
41. Song K, Compaan AM, Chai W, et al. Injectable Gelatin Microgel-Based Composite Ink for 3D Bioprinting in Air. ACS Applied Materials & Interfaces 2020;12(20):22453-22466, doi:10.1021/acsami.0c01497

42. Xin S, Dai J, Gregory CA, et al. Creating Physicochemical Gradients in Modular Microporous Annealed Particle Hydrogels via a Microfluidic Method. Advanced Functional Materials 2020;30(6):1907102, doi:https://doi.org/10.1002/adfm.201907102
43. Pruett LJ, Kenny HL, Swift WM, et al. De novo tissue formation using custom microporous annealed particle hydrogel provides long-term vocal fold augmentation. npj Regenerative Medicine 2023;8(1):10, doi:10.1038/s41536-023-00281-8
44. Truong NF, Kurt E, Tahmizyan N, et al. Microporous annealed particle hydrogel stiffness, void space size, and adhesion properties impact cell proliferation, cell spreading, and gene transfer. Acta Biomaterialia 2019;94(160-172, doi:https://doi.org/10.1016/j.actbio.2019.02.054
45. Seymour AJ, Shin S, Heilshorn SC. 3D Printing of Microgel Scaffolds with Tunable Void Fraction to Promote Cell Infiltration. Advanced Healthcare Materials 2021;10(18):2100644, doi:https://doi.org/10.1002/adhm.202100644
46. Widener AE, Bhatta M, Angelini TE, et al. Guest–host interlinked PEG-MAL granular hydrogels as an engineered cellular microenvironment. Biomaterials Science 2021;9(7):2480-2493, doi:10.1039/D0BM01499K
47. Anderson AR, Nicklow E, Segura T. Particle fraction is a bioactive cue in granular scaffolds. Acta Biomaterialia 2022;150(111-127, doi:https://doi.org/10.1016/j.actbio.2022.07.051
48. Anderson AR, Segura T. Controlling Particle Fraction in Microporous Annealed Particle Scaffolds for 3D Cell Culture. J Vis Exp 2022;188), doi:10.3791/64554
49. Brassard JA, Nikolaev M, Hübscher T, et al. Recapitulating macro-scale tissue self-organization through organoid bioprinting. Nature Materials 2020;20(22-29, doi:10.1038/s41563-020-00803-5
50. Ning L, Mehta R, Cao C, et al. Embedded 3D Bioprinting of Gelatin Methacryloyl-Based Constructs with Highly Tunable Structural Fidelity. ACS Applied Materials & Interfaces 2020;12(40):44563-44577, doi:10.1021/acsami.0c15078
51. Brunel LG, Christakopoulos F, Kilian D, et al. Embedded 3d Bioprinting of Collagen Inks into Microgel Baths to control hydrogel Microstructure and Cell Spreading. Advanced Healthcare Materials 2023;n/a(n/a):2303325, doi:https://doi.org/10.1002/adhm.202303325
52. Jeon O, Lee YB, Jeong H, et al. Individual cell-only bioink and photocurable supporting medium for 3D printing and generation of engineered tissues with complex geometries. The Royal Society of Chemistry: 2019.
53. Oelschlaeger C, Marten J, Péridont F, et al. Imaging of the microstructure of Carbopol dispersions and correlation with their macroelasticity: A micro- and macrorheological study. Journal of Rheology 2022;66(4):749-760, doi:10.1122/8.0000452
54. Morley CD, Ellison ST, Bhattacharjee T, et al. Quantitative characterization of 3D bioprinted structural elements under cell generated forces. Nature Communications 2019;10(1):3029, doi:10.1038/s41467-019-10919-1
55. Solomon MJ, Lu Q. Rheology and dynamics of particles in viscoelastic media. Current Opinion in Colloid & Interface Science 2001;6(5):430-437, doi:https://doi.org/10.1016/S1359-0294(01)00111-X
56. Huang J, Safari R, Fragachan FE. Applications of Self-Degradable Particulate Diverters in Wellbore Stimulations: Hydraulic Fracturing and Matrix Acidizing Case Studies. 2018.
57. Kyrylyuk AV, Philipse AP. Effect of particle shape on the random packing density of amorphous solids. physica status solidi (a) 2011;208(10):2299-2302, doi:https://doi.org/10.1002/pssa.201000361
58. Kalman H. Effect of particle shape on void fraction. Powder Technology 2022;407(117665, doi:https://doi.org/10.1016/j.powtec.2022.117665

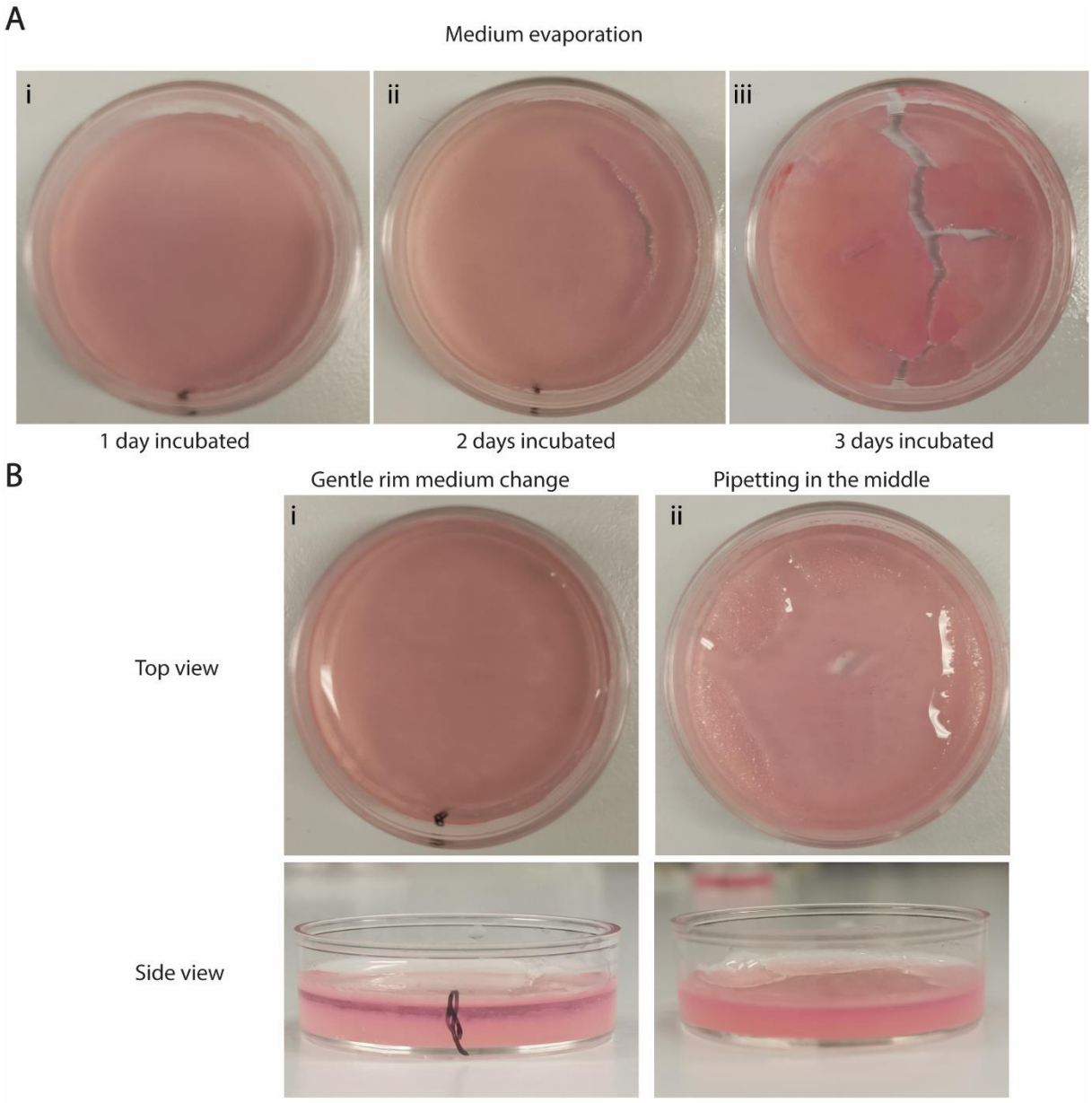

Supplementary Figure 1: Methods to change media without disturbing the suspension. The surface area of the particle suspensions is notably high, and thus evaporation is prominent. (A) When incubated, the suspension dries and needs daily medium change, which for a 35mm dish it was found

to be empirically to be 200µl per day for 4ml of dense particle suspension, which attributes for %5 loss of liquid volume. On the second day of incubation without medium addition, the particle suspension dries and jams irreversibly and no longer behaves as an embedding bath (A.ii-iii). (B) In the case of a petri dish, daily medium supplementation is necessary and it must be done gently by additing the medium on the sides of the dish, in order to not disturb the suspension (B.i). If the medium is pipetted rapidly and on top of the suspension, it will disturb the suspension and result in deformation of printed features and suspension compartments (B.ii). (C) Perfusable chambers are a potential solution for long term incubation of granular suspensions, since the inflow and outflow can remain stable while evaporation can be prevented by not leaving an exposed surface, after injection and printing.

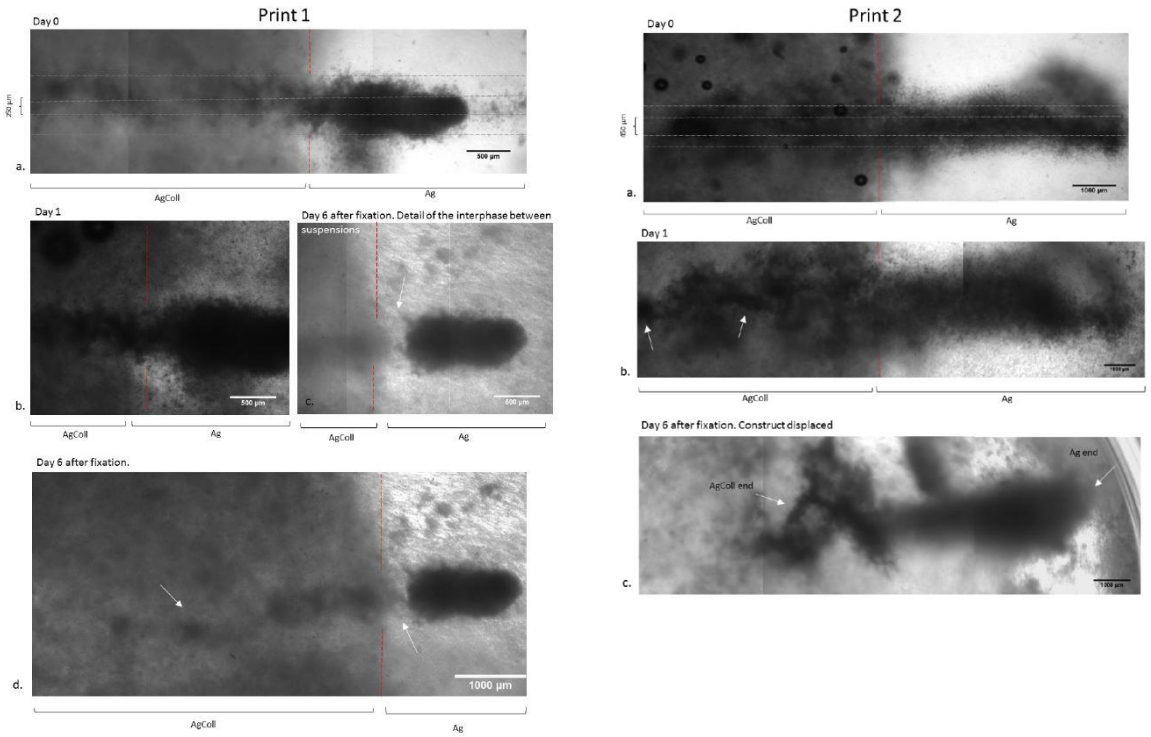

Supplementary Figure 2: Printing in-situ crosslinking inks comprising of cells suspended in 8 mg/ml fibrinogen with a straight nozzle, within a compartmentalized granular bath of agarose-collagen (AgColl) and agarose (Ag) particles, that contains 10U/ml thrombin in the interstitial liquid phase. Using in situ crosslinking for cell suspension inks with a straight nozzle demonstrated mixed results. In the AgColl compartment, the cells spread through the suspension resulting in a loss of feature, while in the Ag phase the cells agglomerate in the fibrin area. The fidelity of the prints is also of low quality since it was demonstrated in Figure 3 that cell suspension inks can be printed with a 90 bent nozzle, and the in situ crosslinking necessitates extensive optimization to mimic hydrogel ink printing. In both print 1 (250µm needle ID) and print 2 (450µm needle ID) the compartments trigger a different behavior to the cells (Print 1 b.,c.,d., compared to Print 2.b.,c.)

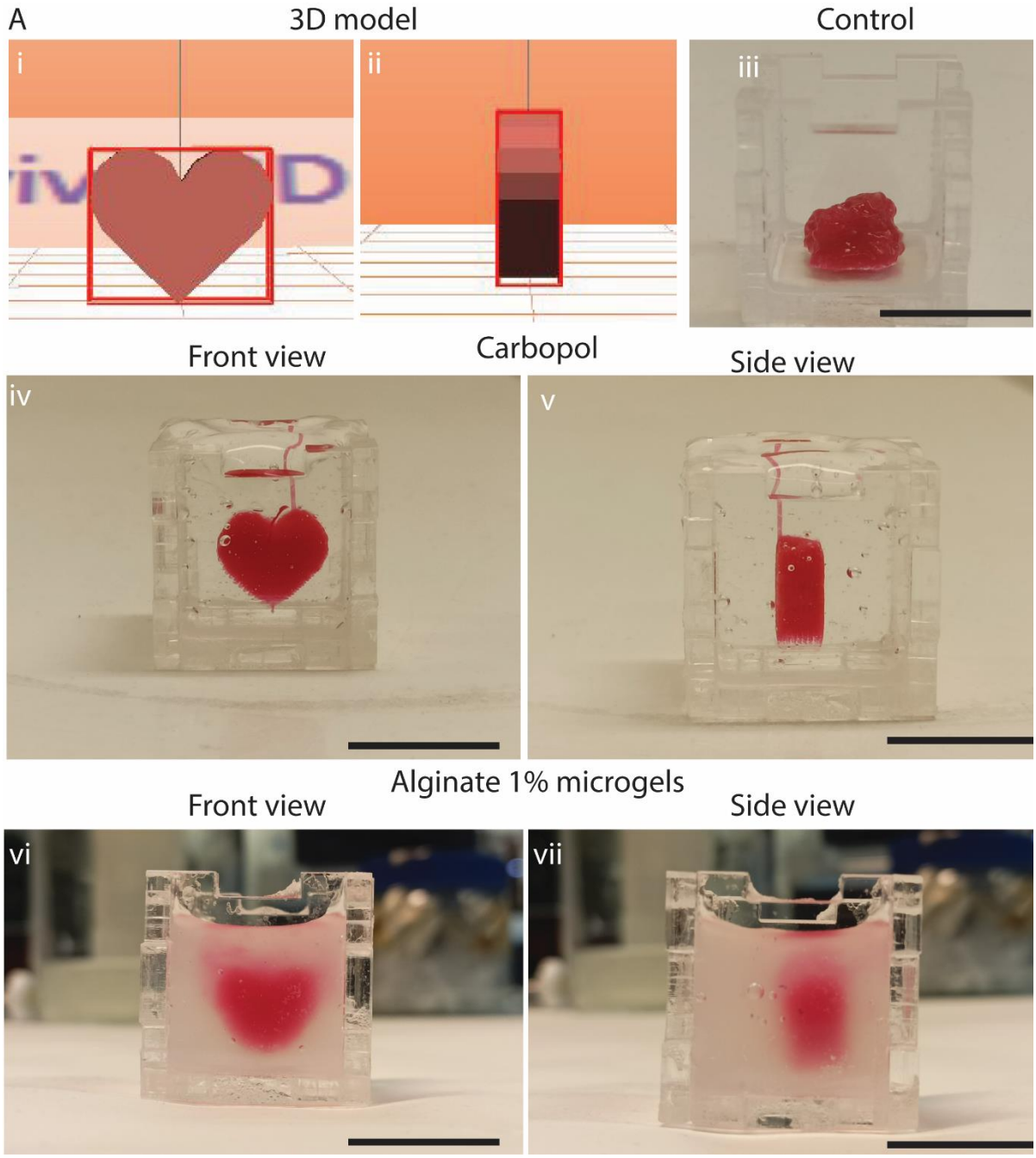

Supplementary Figure 3: Heart shape printed using a 3% xanthan ink with red carmine pigment 1% w/v for visualization. (A) A model of a simple heart shape as seen from the front (i) and side (ii) cannot be printed without support as shown in the control print (iii). Using a carbopol EDT2020 granular support, the fidelity is drastically improved compared to the no-bath control and the printed heart is clearly visible from both the front (Iv) and the side (v). Using Alginate 1% microgels of 150µm, the print fidelity is also drastically improved compared to the no-bath control. However, the slight mismatch between the optical index of the water medium and the alginate particles causes a blur that makes large constructs harder to visualize.